Self-driven configurational dynamics in frustrated spring-mass systems

Ori Saporta-Katz[1] and Avraham Moriel[2,*]
[1]*Computer Science and Applied Mathematics Department, Weizmann Institute of Science, Rehovot 7610001, Israel*
[2]*Chemical and Biological Physics Department, Weizmann Institute of Science, Rehovot 7610001, Israel*

(Received 30 October 2023; accepted 29 January 2024; published 26 February 2024)

Various physical systems relax mechanical frustration through configurational rearrangements. We examine such rearrangements via Hamiltonian dynamics of simple internally stressed harmonic four-mass systems. We demonstrate theoretically and numerically how mechanical frustration controls the underlying potential energy landscape. Then, we examine the harmonic four-mass systems' Hamiltonian dynamics and relate the onset of chaotic motion to self-driven rearrangements. We show such configurational dynamics may occur without strong precursors, rendering such dynamics seemingly spontaneous.

DOI: 10.1103/PhysRevE.109.024219

I. INTRODUCTION

Mechanical frustration and internal stresses endow inanimate and active physical systems with unusual structural features. Internal stresses generate universal low-frequency quasilocalized vibrational modes in amorphous materials and alter their thermodynamical properties [1–5]. Mechanical frustration promotes nonextensive statistics and enables the emergence of complex patterns in spatially extended systems [6–11], and a wide range of conformations and structures for biomolecules and active matter [12,13]. Understanding the role of mechanical frustration in generating these exotic properties is crucial.

Frustrated systems also exhibit diverse dynamical behaviors, including folding and conformational transitions, as means of stress relaxation [14–21]. Such configurational dynamics are either triggered by external driving forces (e.g., mechanical loading) [22–28] or are self-induced [29–36]. However, stress relaxation cannot be entirely attributed to thermally activated or externally driven processes, as stress relaxation can occur even in the absence of external driving or noise [37–45]. Specifically, athermal systems also undergo configurational rearrangements, even though external thermal fluctuations are insufficient to induce such events. While internal stresses clearly play a vital role in self-induced relaxation events [20,46–49], their effects on the underlying energy landscape and on the emerging dynamics remain unclear.

In this work, we use a mechanically frustrated, isolated, spring-mass system [50] to study the role of mechanical frustration on both structural characteristics and emerging dynamics, focusing on self-driven configurational rearrangements. Considering such a simple system allows us to probe generic structural and dynamic effects of internal stresses. We probe the system's Hamiltonian dynamics, rendering all observed behaviors self-driven and not externally induced. We first study how frustration modifies the underlying potential energy landscape, the local and global energetic minima, and the transition state. These modifications affect the system's Hamiltonian dynamics and alter the onset of chaotic motion and configurational rearrangements. Finally, we show such configurational dynamics can occur without strong dynamic precursors.

II. FRUSTRATED SPRING-MASS SYSTEMS

To study internal stress's roles, we look for a simple spring-mass system supporting mechanical frustration. Previous works on the harmonic three-mass systems demonstrated that such a simple system could self-induce rotations [51,52]. As the three masses have to align to allow a force-balanced internally stressed state, we consider here a similar harmonic system composed of fully interacting four-particles (i.e., each particle has three interactions) in two dimensions [50]. Unlike [51,52], we focus on the actual configurational dynamics, and their dependence on the underlying internal stresses. The particles interact via geometrically nonlinear springs of finite rest length $\frac{k}{2}(r_{ij}-L_{ij})^2$, where the spring constant k is set to unity, $r_{ij}\equiv\sqrt{(x_i-x_j)^2+(y_i-y_j)^2}$ is the distance, and L_{ij} is the rest length of the spring between the particles i and j. Using a quadratic potential allows us to study generic features of internally stressed systems, as it is the leading-order contribution of pairwise potentials featuring both repulsive and attractive interactions near the pairwise potential's stable minimum. The total potential energy U is a sum over the pairwise interactions $U=\frac{k}{2}\sum_{\alpha=1}^{6}(r_\alpha-L_\alpha)^2$ (where α runs over all pairs). Figure 1(a) shows a sketch of the system of interest.

The system is stress free when each pairwise interaction exerts zero force. For a stress-free square configuration, $L_{ij}=\ell$ for peripheral pairs and $L_{ij}=\sqrt{2}\ell$ for pairs interacting along the diagonals (ℓ sets the length dimensions). If the net force

*Present address: Department of Mechanical and Aerospace Engineering, Princeton University, New Jersey 08544, USA; amoriel@princeton.edu

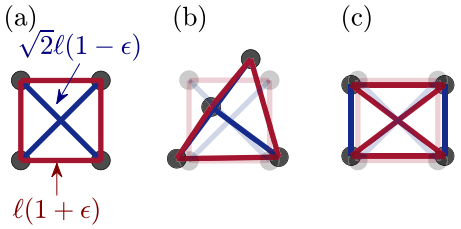

FIG. 1. (a) The square configuration, with the rest lengths of the peripheral springs (red) and diagonal springs (blue) specified as a function of the amplitude of internal stress ϵ and lengthscale ℓ. (b) The transition configuration between the square and rectangle stable mechanical minima. (c) The rectangle stable mechanical minima, where the two blue springs are now on the outer part. All panels are generated using $\epsilon = 0.3$ (and $\ell = 1$), and in panels (b) and (c) the square configuration is reproduced in the background for comparison.

over each particle vanishes, while the pairwise forces are *nonzero*, the system is mechanically frustrated [1,50,53,54]. The four-mass system allows a frustrated state once the individual springs are *not* at their rest lengths. We obtain such a state by changing the spring rest lengths to $L_{ij} = \ell(1+\epsilon)$ for peripheral pairs, and $L_{ij} = \sqrt{2}\ell(1-\epsilon)$ along the diagonals [55], as shown in Fig. 1(a). We set ℓ to unity, such that the dimensionless ϵ captures the internal stress amplitude.

Taken together with the kinetic energy $K = \frac{1}{2m}\sum_{i=1}^{4} p_i^2$ of the four-mass system (i runs over the four particles, $p_i \equiv |\boldsymbol{p}_i|$, $\boldsymbol{p}_i = (p_i^x, p_i^y)$, and m set to unity), the system's Hamiltonian $\mathcal{H}$ is [56]

$$\mathcal{H} = K + U. \tag{1}$$

The Hamiltonian dynamics of the system conserve the total energy, such that possible configurational changes are only self-induced (and are not externally triggered).

III. MECHANICAL FRUSTRATION MODIFIES THE ENERGY LANDSCAPE

We first focus on the implications of mechanical frustration on the underlying potential energy U. The potential energy at the square configuration U_S changes quadratically with ϵ, as shown in Fig. 2(a). Expanding U perturbatively around the square geometry, we obtain the Hessian $\boldsymbol{\mathcal{M}} \equiv \frac{\partial^2 U}{\partial \boldsymbol{r} \partial \boldsymbol{r}}$, its eigenmodes $\boldsymbol{\psi}$, and their respective frequencies ω via the eigenvalue equation $\boldsymbol{\mathcal{M}}\boldsymbol{\psi}_i = \omega_i^2 \boldsymbol{\psi}_i$ (without summation). The lowest frequency at the square configuration $\omega_S^{\min}$ changes with ϵ as shown in Fig. 2(b), and becomes negative at $|\epsilon| = 1$ [50], implying the square configuration becomes unstable. In what follows, we study the system in the stable range $|\epsilon| < 1$.

While the square configuration is stable for $|\epsilon| < 1$, it does not imply that it is the *only* energetic minimum in the entire energy landscape. A particle swap along the two diagonals will result in a geometrically identical square configuration; swapping any peripheral pair will yield a rectangular shape with potential energy U_R and minimal frequency $\omega_R^{\min}$ as sketched in Fig. 1(c). This configuration is potentially another energetic minimum [55]. We numerically test and verify that the rectangular configuration serves as an additional minimum by initiating the four masses at random configurations and minimizing their potential energy to recover the closest minimum. The results obtained from this numerical procedure exactly match our analytical calculations, as shown in Fig. 2(a).

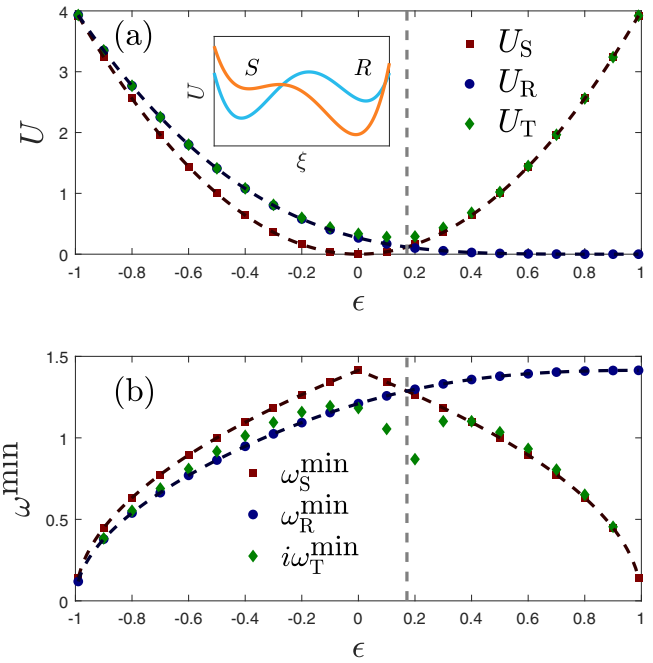

FIG. 2. (a) The potential energy values at the square configuration U_S, the rectangular configuration U_R, and the transition state U_T. The U_S, U_R data are obtained from random configuration sampling and numerical minimization of the potential energy. The U_T data are obtained via the nudged elastic band algorithm between the square and rectangle configuration. Dashed lines indicate the theoretically predicted values [55], and the vertical dashed line denotes the critical ϵ_* value where the global minimum switches between the square geometry ($\epsilon < \epsilon_*$) and the rectangular configuration ($\epsilon > \epsilon_*$). Inset: a sketch of the potential energy landscape versus the reaction coordinate ξ, showing schematically that for $\epsilon < \epsilon_*$ the square is a global minimum (blue), and for $\epsilon > \epsilon_*$ the rectangular configuration becomes the global one (orange). (b) The minimal frequencies at the square and rectangular minima and the divergence rate at the transition configurations. $\omega_S^{\min}$ and $\omega_R^{\min}$ are associated with the minimal oscillation frequencies around the square and rectangle configurations, while, for the transition state, $i\omega_T^{\min}$ corresponds to the divergence rate from the transition state.

For ϵ values below a critical value [55] $\epsilon_* = 3 - 2\sqrt{2}$ the square geometry serves as a *global* minimum of the potential energy landscape, while for $\epsilon > \epsilon_*$ the rectangle configuration becomes the *global* minimum, and the initial square geometry turns into a *local* minimum [interestingly $\omega_R^{\min}$ crosses $\omega_S^{\min}$ at ϵ_*, shown in Fig. 2(b)]. The value of ϵ_* is plotted as a dashed vertical line in Fig. 2(a), and we sketch this scenario in the inset of Fig. 2(a).

The existence of several energetic minima implies that transition states exist in between. The transition state between the square and rectangular geometry resembles the one sketched in Fig. 1(b), where the top two particles swap. To detect and probe the transition state between the two

minima, we employ the nudged elastic band algorithm [57,58] followed by force amplitude minimization. We plot the potential energy at the transition state U_T in Fig. 2(a). For $\epsilon < \epsilon_*$ the transition potential energy is well approximated by U_R, while for $\epsilon > \epsilon_*$ it is closer to U_S (though $U_T > U_S, U_R$).

At the transition state, the smallest eigenvalue is negative by definition [59]. We plotted the associated frequency $i\omega_T^{\min}$ in Fig. 2(b). Unlike the stable mechanical minima, this value corresponds to a divergence rate, not an oscillation frequency. Once the system is provided with sufficient energy, it can pass between the two minima. The internal stress level changes the potential energy minima (local and global) and the potential energy barrier. Thus, we hypothesize mechanical frustration will also play a crucial role in the Hamiltonian dynamics of such a system, specifically in the onset of chaotic motion and configurational rearrangements.

IV. HAMILTONIAN DYNAMICS AND CHAOTIC MOTION

So far, we considered internal stresses' effects on the underlying potential energy landscape. Which special dynamical behaviors emerge due to mechanical frustration? To probe the intrinsic dynamics of the frustrated spring-mass systems, we consider the Hamiltonian dynamics governed by Eq. (1). We initialize the system at its internally stressed, square configuration and set the initial velocities randomly. We remove any linear and angular momentum from the initial velocities and ensure that the total excess kinetic energy provided to the system is E_* [55]. Overall, the initial configuration corresponds to a potential energy $U_S(\epsilon)$, and an initial kinetic energy $K = E_*$ (with no linear and angular momentum). We probe the self-driven dynamics via measuring the maximal Lyapunov exponent $\lambda_{\max}$ [59,60] numerically [61,62], at the end of our simulations (well after the initial transient dynamics [55]). We plot $\lambda_{\max}$ averaged over an ensemble of 100 realizations in Fig. 3(a).

At low E_* values, the system oscillates around the square configuration (as it is a stable mechanical minimum [56,59], according to the KAM theory [63]), and $\lambda_{\max}$ is expected to be low [52,59]. At high E_*, the values of L_{ij} become irrelevant, and the system is expected to exhibit regular dynamics again [52]. For intermediate excess energies, $\lambda_{\max}$ peaks approximately at the energy needed to compress a single bond (varying with ϵ). These results are qualitatively similar to those of the harmonic three-mass system [52].

Surprisingly, at low energies and for $\epsilon > \epsilon_*$, $\lambda_{\max}$ plateaus at energy scales lower than those associated with a single bond compression, as shown in Fig. 3(a). As $\epsilon \to 1$ the plateau persists to lower energy scales. This peculiar behavior has not been observed in the case of a triangle [52] and seems to emerge specifically due to mechanical frustration (absent from the system considered in [51,52]). Intrigued by this phenomenon, we repeated the same procedure, initializing the system at the rectangular configuration. This results in $\lambda_{\max}$ shown in Fig. 3(b). Now we observe a plateau for sufficiently low ϵ values (we discuss the appearance of plateaus at higher ϵ values in [55]). The $\lambda_{\max}$ plateaus seem to correlate with the global-to-local transition of the two configurations. We hypothesize the transition state governs this *dynamical* observable.

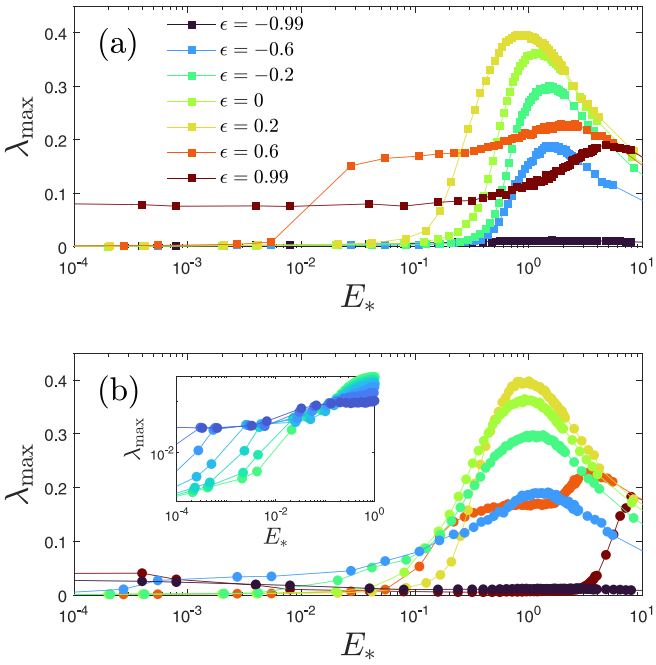

FIG. 3. (a) The maximal Lyapunov exponents $\lambda_{\max}$ for trajectories initiated with the square geometry, for different ϵ values and wide excess energy E_* ranges (each point corresponds to ensemble average over 100 realizations). Above ϵ_*, $\lambda_{\max}$ plateaus to a finite value at low E_*. (b) $\lambda_{\max}$ for trajectories initiated with the rectangle geometry, for ϵ values and energy range as in panel (a) (each point corresponds to ensemble average over 100 realizations). A $\lambda_{\max}$ plateau occurs at $\epsilon < \epsilon_*$ values, where the rectangular geometry is a local minimum of the potential energy landscape. Inset: a log-log plot zoomed-in on the plateau at low E_* values for ϵ between -0.8 (blue) and -0.2 (green).

At low energies, the system's trajectories occupy phase space regions close to the mechanically stable states. Such trajectories describe the system's oscillations around the stable mechanical minimum. At some stage, E_* is sufficient for the system to pass over the transition state, resulting in configurational rearrangement; the available phase space changes dramatically as it now includes several stable minima and saddles. We hypothesize that the saddles act as effective scatterers of the trajectories, causing them to diverge from one another, increasing the Lyapunov exponent [59]. Further increasing E_*, the phase space volume includes more saddles and minima, possibly scattering the trajectories even more strongly. Eventually, all minima and saddles are included, and the phase-space volume increases trivially with increased available energy.

To test this argument, we focus on the transition between the square and rectangular configurations. We consider trajectories with ϵ values in which the initial configuration is the *local* minimum, as shown in Figs. 4(a) and 4(b). Once we rescale E_* by the relative barrier energy $\Delta U_{T-S} \equiv U_T - U_S$ ($\Delta U_{T-R} \equiv U_T - U_R$) for the square (rectangular) trajectories, the initial increase in $\lambda_{\max}$ collapses, as shown in Fig. 4(c). Then, we approximate the value of $\lambda_{\max}$ at the plateau, $\lambda_{\max}^p$, by averaging over the first seven entries above the barrier energy. We plot the resulting $\lambda_{\max}^p$ versus $i\omega_T^{\min}$ in Fig. 4(d),

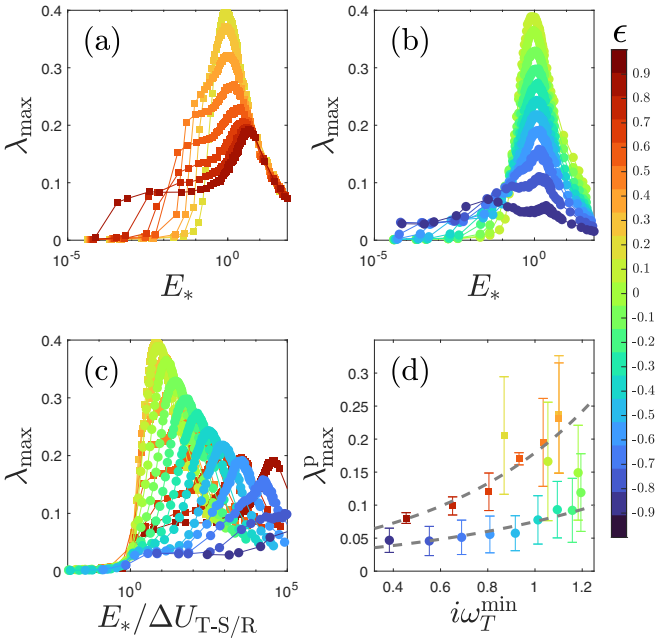

FIG. 4. (a) $\lambda_{\max}$ from the square trajectories (with $\epsilon > \epsilon_*$) versus E_*. (b) $\lambda_{\max}$ form the rectangular trajectories (with $\epsilon < \epsilon_*$) vs E_*. (c) The same $\lambda_{\max}$ from panels (a) and (b) [□ corresponds to the square data of panel (a) and ○ corresponds to the rectangular data from panel (b)] vs E_* rescaled by the barrier energy $\Delta U_{\text{T-S}}$ for data from panel (a), and $\Delta U_{\text{T-R}}$ for data from panel (b). (d) The approximated plateau value of the Lyapunov exponent $\lambda^p_{\max}$ (an average over the first seven points above the barrier energy) vs $i\omega^{\min}_{\text{T}}$ (error bars indicate the standard deviation of the seven points). For well-approximated plateaus (small error bars), $\lambda^p_{\max}$ forms a function of $i\omega^{\min}_T$ (the two gray exponential curves serve as a guide to the eye). □ corresponds to the square data and ○ corresponds to the rectangular data. The color bar shows the ϵ values used in the four panels.

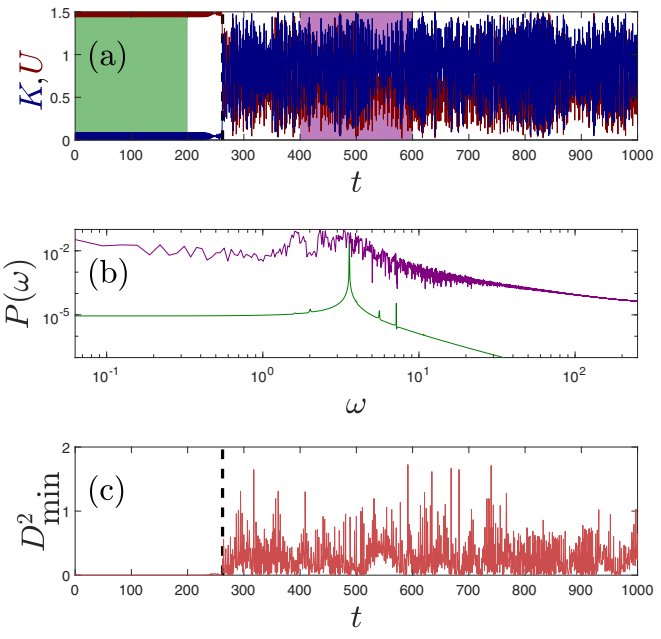

FIG. 5. (a) Kinetic (blue) and potential (red) energies as a function of time for $\epsilon = 0.3$ and $E_* \simeq 0.08$ ($\Delta U_{\text{T-S}} \simeq 0.07$). A vertical black dashed line marks the first crossing between U and K. Early-time and late-time regions are marked with green- and purple-shaded regions, respectively. (b) The power spectrum of the early-time and late-time shaded regions of (a). The early-time power spectrum of U includes discrete peaks representative of regular dynamics, while the late-time power spectrum contains contributions at all frequencies. (c) $D^2_{\min}$ measure of nonaffine motion as a function of time for the same trajectory. The moment of the first crossing is marked with a vertical black dashed line, indicating that the crossing of U and K is accompanied by a large nonaffine motion.

demonstrating the functional relation $\lambda^p_{\max}(i\omega^{\min}_{\text{T}})$ for well-detected plateaus [59]. The results of Figs. 4(c) and 4(d) demonstrate the relation between the transition state, which is a *potential energy landscape* property, and an increased Lyapunov exponent, which is a *dynamical* observable [64–66].

V. CONFIGURATIONAL DYNAMICS

The Lyapunov exponents' plateaus emerging at energies above the barrier energy hint that at least some trajectories within the ensemble are configurationally rearranged. Next, we would like to dynamically follow individual trajectories, looking for dynamical precursors for configurational rearrangements. To do that, we follow trajectories originating from the square configuration for $\epsilon > \epsilon_*$, with E_* slightly above $\Delta U_{\text{T-S}}$ to detect self-driven configurational rearrangements. The system oscillates around the initial configuration until it passes over the energetic barrier, releasing its stored potential energy. These dynamics correspond to configurational rearrangements like that shown in Fig. 1.

Are there any precursors to these rearrangements? We plot various dynamic measurements from an example trajectory in Fig. 5. Figure 5(a) shows K and U throughout the dynamics, revealing the finite-time release of the initially stored potential energy, as indicated by the vertical dashed line. This release signifies passing away from the square energy basin to other regions in phase space. The system oscillates uniformly until it passes over the energetic barrier, after which the dynamics become irregular.

To further examine the dynamics before and after the barrier crossing, we analyze the power spectrum of U in the early and late stages of the simulations in Fig. 5(b) [corresponding to the shaded regions in Fig. 5(a)]. The early-time power spectrum shows discrete peaks and does not hint at the impending configurational change. After crossing the energetic barrier, various frequencies fill the power spectrum, indicating that the trajectory becomes irregular, and the total energy was redistributed (reminiscent of thermalization [67]).

We also measured the degree of nonaffine motion via the $D^2_{\min}$ measure [22] in Fig. 5(c). The $D^2_{\min}$ measure peaks at the first crossing of U and K, indicating that passing from the square energy basin to the outer phase-space is associated with a nonaffine deformation of the system, suggesting that the system underwent a dramatic configurational rearrangement to pass over the barrier. While other dynamical behaviors are possible [55], we have not observed strong dynamical precursors to such configurational changes, rendering these self-driven events "spontaneous" [20].

VI. DISCUSSION

We studied self-driven configurational dynamics in frustrated spring four-mass systems. Changing the internal stress amplitude ϵ varied the springs' rest lengths and modified the stable mechanical minima and the transition states between them. These modifications yielded unique Lyapunov exponent plateaus. The plateaus arise at energies comparable to the barrier energies $U_{\mathrm{T}} - U_{\mathrm{S/R}}$ and are affected by the eigenvalue associated with the saddle's most unstable direction. Finally, we have demonstrated how trajectories with sufficient excess energy could seem completely regular before undergoing configurational changes and overcoming the energetic barrier.

The isolated spring-mass systems considered above allowed us to vary the internal stress continuously and study the emerging self-driven dynamics. This systematic variation allowed us to relate the emerging plateau in $\lambda^{p}_{\max}$ with $i\omega_T^{\min}$, which is unavailable once a specific molecule or material is considered [64–66]. Mathematically, this demonstrates the effects of saddle points on $\lambda_{\max}$ when the underlying energy landscape is complex (e.g., in mixed systems).

The isolated system considered above is not spatially extended, preventing us from further exploring the spatial signatures of such configurational dynamics [20,37,39]. Spatially extended systems undergoing configurational rearrangements can divert and spread the released energy to other system parts or an external bath, possibly inducing avalanches [23,38,45]. The isolated four-mass system cannot support this behavior. We suspect that embedding a mechanically frustrated element within a stress-free spatially extended system will suppress the configurational dynamics observed above (as these will be more energetically costly). Including positional disordered, internally stressed elements may lower the energetic barriers and enable studying the spatiotemporal dynamics triggered by self-induced configurational dynamics.

ACKNOWLEDGMENTS

We thank Yuri Lubomirsky for his insightful comments and discussions, and Dor Shohat, Yoav Lahini, and Eran Bouchbinder for commenting on the manuscript. O.S.K. acknowledges the support of a research grant from the Yotam Project and the Weizmann Institute Sustainability and Energy Research Initiative; and the support of the Séphora Berrebi Scholarship in Mathematics. A.M. acknowledges support from the Minerva Foundation (with funding from the Federal German Ministry for Education and Research), the Ben May Center for Chemical Theory and Computation, and the Harold Perlman Family.

O.S.K. and A.M. designed the research. A.M. performed numerical simulations. O.S.K. and A.M. performed theoretical calculations and wrote the manuscript.

[1] S. Alexander, Amorphous solids: Their structure, lattice dynamics and elasticity, Phys. Rep. **296**, 65 (1998).

[2] F. Wang, S. Mamedov, P. Boolchand, B. Goodman, and M. Chandrasekhar, Pressure Raman effects and internal stress in network glasses, Phys. Rev. B **71**, 174201 (2005).

[3] M. Wyart, On the rigidity of amorphous solids, Ann. Phys. (France) **30**, 1 (2005).

[4] E. Lerner and E. Bouchbinder, Frustration-induced internal stresses are responsible for quasilocalized modes in structural glasses, Phys. Rev. E **97**, 032140 (2018).

[5] H. Mizuno and A. Ikeda, Phonon transport and vibrational excitations in amorphous solids, Phys. Rev. E **98**, 062612 (2018).

[6] S. Meiri and E. Efrati, Cumulative geometric frustration in physical assemblies, Phys. Rev. E **104**, 054601 (2021).

[7] S. Meiri and E. Efrati, Cumulative geometric frustration and superextensive energy scaling in a nonlinear classical XY-spin model, Phys. Rev. E **105**, 024703 (2022).

[8] S. Meiri and E. Efrati, Bridging cumulative and noncumulative geometric frustration response via a frustrated N-state spin system, Phys. Rev. Res. **4**, 033104 (2022).

[9] Y. Han, Y. Shokef, A. M. Alsayed, P. Yunker, T. C. Lubensky, and A. G. Yodh, Geometric frustration in buckled colloidal monolayers, Nature (London) **456**, 898 (2008).

[10] S. H. Kang, S. Shan, A. Košmrlj, W. L. Noorduin, S. Shian, J. C. Weaver, D. R. Clarke, and K. Bertoldi, Complex ordered patterns in mechanical instability induced geometrically frustrated triangular cellular structures, Phys. Rev. Lett. **112**, 098701 (2014).

[11] H. Aharoni, J. M. Kolinski, M. Moshe, I. Meirzada, and E. Sharon, Internal stresses lead to net forces and torques on extended elastic bodies, Phys. Rev. Lett. **117**, 124101 (2016).

[12] V. Nier, S. Jain, C. T. Lim, S. Ishihara, B. Ladoux, and P. Marcq, Inference of internal stress in a cell monolayer, Biophys. J. **110**, 1625 (2016).

[13] F. Burla, Y. Mulla, B. E. Vos, A. Aufderhorst-Roberts, and G. H. Koenderink, From mechanical resilience to active material properties in biopolymer networks, Nat. Rev. Phys. **1**, 249 (2019).

[14] C. D. Modes, M. Warner, C. Sánchez-Somolinos, L. T. De Haan, and D. Broer, Mechanical frustration and spontaneous polygonal folding in active nematic sheets, Phys. Rev. E **86**, 060701(R) (2012).

[15] Y. Zhang and O. K. Dudko, A transformation for the mechanical fingerprints of complex biomolecular interactions, Proc. Natl. Acad. Sci. USA **110**, 16432 (2013).

[16] C. A. Pierse and O. K. Dudko, Distinguishing signatures of multipathway conformational transitions, Phys. Rev. Lett. **118**, 088101 (2017).

[17] L. F. Milles, E. M. Unterauer, T. Nicolaus, and H. E. Gaub, Calcium stabilizes the strongest protein fold, Nat. Commun. **9**, 4764 (2018).

[18] L. Tskhovrebova, J. Trinick, J. A. Sleep, and R. M. Simmons, Elasticity and unfolding of single molecules of the giant muscle protein titin, Nature (London) **387**, 308 (1997).

[19] Q. Guo, Z. Chen, W. Li, P. Dai, K. Ren, J. Lin, L. A. Taber, and W. Chen, Mechanics of tunable helices and geometric frustration in biomimetic seashells, Europhys. Lett. **105**, 64005 (2014).

[20] O. Lieleg, J. Kayser, G. Brambilla, L. Cipelletti, and A. R. Bausch, Slow dynamics and internal stress relaxation in bundled cytoskeletal networks, Nat. Mater. **10**, 236 (2011).

[21] Y. Zhang, D. S. W. Lee, Y. Meir, C. P. Brangwynne, and N. S. Wingreen, Mechanical frustration of phase separation in the cell nucleus by chromatin, Phys. Rev. Lett. **126**, 258102 (2021).
[22] M. L. Falk and J. S. Langer, Dynamics of viscoplastic deformation in amorphous solids, Phys. Rev. E **57**, 7192 (1998).
[23] J. Lauridsen, M. Twardos, and M. Dennin, Shear-induced stress relaxation in a two-dimensional wet foam, Phys. Rev. Lett. **89**, 098303 (2002).
[24] I. Cohen, T. G. Mason, and D. A. Weitz, Shear-induced configurations of confined colloidal suspensions, Phys. Rev. Lett. **93**, 046001 (2004).
[25] M. Dennin, Statistics of bubble rearrangements in a slowly sheared two-dimensional foam, Phys. Rev. E **70**, 041406 (2004).
[26] C. E. Maloney, and A. Lemaître, Amorphous systems in athermal, quasistatic shear, Phys. Rev. E **74**, 016118 (2006).
[27] P. Schall, D. A. Weitz, and F. Spaepen, Structural rearrangements that govern flow in colloidal glasses, Science **318**, 1895 (2007).
[28] M. Lundberg, K. Krishan, N. Xu, C. S. O'Hern, and M. Dennin, Reversible plastic events in amorphous materials, Phys. Rev. E **77**, 041505 (2008).
[29] I. M. Hodge, Physical aging in polymer glasses, Science **267**, 1945 (1995).
[30] J. C. Phillips, Stretched exponential relaxation in molecular and electronic glasses, Rep. Prog. Phys. **59**, 1133 (1996).
[31] B. Abou, D. Bonn, and J. Meunier, Aging dynamics in a colloidal glass, Phys. Rev. E **64**, 021510 (2001).
[32] G. B. McKenna, Diverging views on glass transition, Nat. Phys. **4**, 673 (2008).
[33] B. X. Feng, X. N. Mao, G. J. Yang, L. L. Yu, and X. D. Wu, Residual stress field and thermal relaxation behavior of shot-peened TC4-DT titanium alloy, Mater. Sci. Eng. A **512**, 105 (2009).
[34] S. Moreno-Flores, R. Benitez, M. dM Vivanco, and J. L. Toca-Herrera, Stress relaxation microscopy: Imaging local stress in cells, J. Biomech. **43**, 349 (2010).
[35] R. C. Welch, J. R. Smith, M. Potuzak, X. Guo, B. F. Bowden, T. J. Kiczenski, D. C. Allan, E. A. King, A. J. Ellison, and J. C. Mauro, Dynamics of glass relaxation at room temperature, Phys. Rev. Lett. **110**, 265901 (2013).
[36] J. C. Qiao, Y. J. Wang, L. Z. Zhao, L. H. Dai, D. Crespo, J. M. Pelletier, L. M. Keer, and Y. Yao, Transition from stress-driven to thermally activated stress relaxation in metallic glasses, Phys. Rev. B **94**, 104203 (2016).
[37] L. Cipelletti, S. Manley, R. C. Ball, and D. A. Weitz, Universal aging features in the restructuring of fractal colloidal gels, Phys. Rev. Lett. **84**, 2275 (2000).
[38] J. Song, Q. Zhang, F. de Quesada, M. H. Rizvi, J. B. Tracy, J. Ilavsky, S. Narayanan, E. Del Gado, R. L. Leheny, N. Holten-Andersen, and G. H. McKinley, Microscopic dynamics underlying the stress relaxation of arrested soft materials, Proc. Natl. Acad. Sci. USA **119**, e2201566119 (2022).
[39] L. Cipelletti, L. Ramos, S. Manley, E. Pitard, D. A. Weitz, E. E. Pashkovski, and M. Johansson, Universal non-diffusive slow dynamics in aging soft matter, Faraday Discuss. **123**, 237 (2003).
[40] J. P. Bouchaud, and E. Pitard, Anomalous dynamical light scattering in soft glassy gels, Eur. Phys. J. E **6**, 231 (2001).
[41] Y. Lahini, O. Gottesman, A. Amir, and S. M. Rubinstein, Nonmonotonic aging and memory retention in disordered mechanical systems, Phys. Rev. Lett. **118**, 085501 (2017).
[42] Y. Lahini, S. M. Rubinstein, and A. Amir, Crackling noise during slow relaxations in crumpled sheets, Phys. Rev. Lett. **130**, 258201 (2023).
[43] P. Sollich, F. Lequeux, P. Hébraud, and M. E. Cates, Rheology of soft glassy materials, Phys. Rev. Lett. **78**, 2020 (1997).
[44] A. S. Balankin, O. Susarrey Huerta, F. Hernández, Méndez, and J. Patiño Ortiz, Slow dynamics of stress and strain relaxation in randomly crumpled elasto-plastic sheets, Phys. Rev. E **84**, 021118 (2011).
[45] D. Shohat, Y. Friedman, and Y. Lahini, Logarithmic aging via instability cascades in disordered systems, Nat. Phys. **19**, 1890 (2023).
[46] K. González-López, M. Shivam, Y. Zheng, M. Pica Ciamarra, and E. Lerner, Mechanical disorder of sticky-sphere glasses. I. Effect of attractive interactions, Phys. Rev. E **103**, 022605 (2021).
[47] K. González-López, M. Shivam, Y. Zheng, M. Pica Ciamarra, and E. Lerner, Mechanical disorder of sticky-sphere glasses. II. Thermomechanical inannealability, Phys. Rev. E **103**, 022606 (2021).
[48] E. Lerner, and E. Bouchbinder, Effect of instantaneous and continuous quenches on the density of vibrational modes in model glasses, Phys. Rev. E **96**, 020104(R) (2017).
[49] G. Kapteijns, D. Richard, E. Bouchbinder, T. B. Schrøder, J. C. Dyre, and E. Lerner, Does mesoscopic elasticity control viscous slowing down in glassforming liquids? J. Chem. Phys. **155**, 074502 (2021).
[50] A. Moriel, Internally stressed and positionally disordered minimal complexes yield glasslike nonphononic excitations, Phys. Rev. Lett. **126**, 088004 (2021).
[51] O. Saporta Katz, and E. Efrati, Self-driven fractional rotational diffusion of the harmonic three-mass system, Phys. Rev. Lett. **122**, 024102 (2019).
[52] O. Saporta Katz, and E. Efrati, Regular regimes of the harmonic three-mass system, Phys. Rev. E **101**, 032211 (2020).
[53] X. Mao, and T. C. Lubensky, Maxwell lattices and topological mechanics, Annu. Rev. Condens. Matter Phys. **9**, 413 (2018).
[54] T. C. Lubensky, C. L. Kane, X. Mao, A. Souslov, and K. Sun, Phonons and elasticity in critically coordinated lattices, Rep. Prog. Phys. **78**, 073901 (2015).
[55] See Supplemental Material at http://link.aps.org/supplemental/10.1103/PhysRevE.109.024219 for additional information regarding the construction of the square geometry, analytical derivation of the potential energies of the square and rectangular configurations, simulation specifications, discussion of the additional Lyapunov exponent plateaus, and additional dynamical behaviors exhibited, which includes Refs. [4,50,56,61–63,68–71].
[56] L. D. Landau and E. M. Lifshitz, *Mechanics*, Landau and Lifshitz Course of Theoretical Physics Vol. 1 (Elsevier, Amsterdam, 1976).
[57] E. B. Tadmor and R. E. Miller, *Modeling Materials: Continuum, Atomistic and Multiscale Techniques* (Cambridge University Press, Cambridge, 2011).
[58] D. Wales, *Energy Landscapes: Applications to Clusters, Biomolecules and Glasses* (Cambridge University Press, Cambridge, 2003).

[59] S. H. Strogatz, *Nonlinear Dynamics and Chaos with Student Solutions Manual: With Applications to Physics, Biology, Chemistry, and Engineering* (CRC, Boca Raton, 2018).

[60] K. Ramasubramanian, and M. S. Sriram, A comparative study of computation of Lyapunov spectra with different algorithms, Physica D: Nonlinear Phenom. **139**, 72 (2000).

[61] A. Wolf, J. B. Swift, H. L. Swinney, and J. A. Vastano, Determining Lyapunov exponents from a time series, Physica D: Nonlinear Phenom. **16**, 285 (1985).

[62] V. Govorukhin, Calculation Lyapunov exponents for ODE, MATLAB Central File Exchange, 2023.

[63] A. J. Lichtenberg and M. A. Lieberman, *Regular and Chaotic Dynamics* (Springer, Berlin, 2013).

[64] G. Wu, *Nonlinearity and Chaos in Molecular Vibrations* (Elsevier, Amsterdam, 2005).

[65] J. Huang, and G. Wu, Dynamical potential approach to DCO highly excited vibration, Chem. Phys. Lett. **439**, 231 (2007).

[66] F. Chao, and W. Guo-Zhen, Dynamical potential approach to dissociation of H–C bond in HCO highly excited vibration, Chin. Phys. B **18**, 130 (2009).

[67] M. Onorato, L. Vozella, D. Proment, and Y. V. Lvov, Route to thermalization in the α-Fermi-Pasta-Ulam system, Proc. Natl. Acad. Sci. USA **112**, 4208 (2015).

[68] Wolfram Research Inc., *Mathematica*, Version 13.3, Champaign, IL, 2023.

[69] G. Strang, *Introduction to Linear Algebra* (Cambridge University Press, Cambridge, 2016).

[70] The MathWorks Inc., MATLAB, Version R2022b, Natick, Massachusetts, 2022.

[71] F. Beron-Vera, Symplectic integrators, MATLAB Central File Exchange, 2023.